Journal of
Materials Chemistry C

Accepted Manuscript

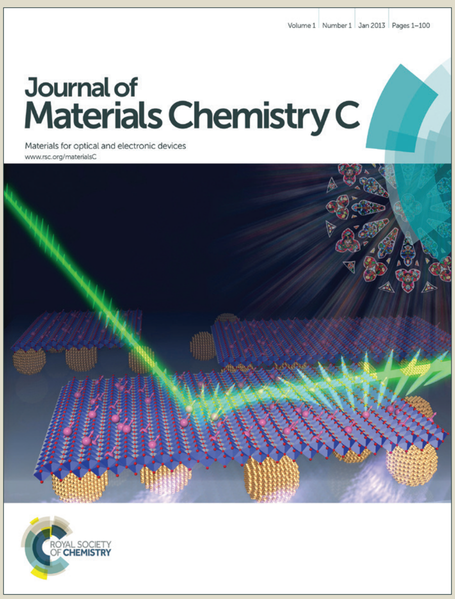

Journal of Materials Chemistry C RSCPublishing

ARTICLE

Cite this: DOI: 10.1039/x0xx00000x

Received 00th January 2012,
Accepted 00th January 2012

DOI: 10.1039/x0xx00000x

www.rsc.org/

Ferroelectric liquid-crystalline semiconductors based on a phenylterthiophene skeleton: Effect of introduction of oligosiloxane moieties and photovoltaic effect

Yusuke Funatsu,[a] Akinari Sonoda,[b] and Masahiro Funahashi*[a]

Ferroelectric liquid-crystalline phenylterthiophene derivatives bearing a decenyl group, disiloxane chain, and tetracyclosiloxane ring were synthesized. These compounds exhibited a chiral smectic C (SmC*) phase. The spontaneous polarizations of the compounds exceeded 50 $nCcm^{-2}$. The hole mobilities determined by the time-of-flight method were on the order of 1×10^{-4} $cm^2V^{-1}s^{-1}$. The compound with a decenyl group exhibited an anomalous photovoltaic effect in the SmC* phase. Notably, even the compound bearing a bulky cyclotetrasiloxane ring exhibited an enatiotropic SmC* phase. Anomalous photovoltaic effects were observed in the SmC* phase of these compounds, although the conversion efficiency was lower than 0.01%.

Introduction

Liquid-crystalline (LC) semiconductors exhibit high carrier mobilities exceeding 0.1 $cm^2V^{-1}s^{-1}$.[1] The closed and ordered molecular packing structures in LC phases enhance the electronic charge carrier transport in columnar[2] and smectic phases.[3] Solution-processable LC oligothiophene and fluorene derivatives have been applied in field-effect transistors (FETs)[4] and polarized electroluminescence devices,[5] respectively. Solar cells based on LC phthalocyanine and LC diketopyrrolopyrrole have also been reported.[6] LC semiconductors are soft and consequently more suitable for flexible devices than crystalline semiconductors.[4e]

Moreover, the introduction of proper side chains and functional groups into π-conjugated cores promotes nanosegregation.[7a,b] Three-dimensional network structures are formed in the bicontinuous cubic phase of oligothiophene with a polycatenar structure.[7c] LC phenylterthiophene derivatives bearing imidazolium moieties exhibit electrochromism in the smectic phase.[7d,e] Perylene tetracarboxylic bisimide derivatives bearing oligosiloxane moieties exhibit nanosegregated columnar and lamellar phases at room temperature.[8]

Some chiral LC molecules exhibit a ferroelectric chiral smectic C (SmC*) phase.[9a,b] In the SmC* phase, the LC molecules tilt from the layer normal and form a helical structure without an electric field. Under a DC bias, the helical structure disappears and the molecular dipoles orient in the direction of the electric field, resulting in spontaneous polarization. By reversing the polarity of the electric field, the director of the LC molecules can be changed rapidly.[9c] Applications in displays have been studied extensively.[9d]

LC semiconductors exhibiting a SmC* phase are expected to facilitate novel electronic functions based on the coupling between electronic charge carrier transport and internal electric fields based on ferroelectricity. The first example of a ferroelectric LC semiconductor was reported by Hanna and Funahashi.[10] However, the spontaneous polarization was lower than 1 $nCcm^{-2}$. No phenomena brought on by the synergism between carrier transport and ferroelectricity has been observed in ferroelectric LCs.

In this study, we synthesized LC phenylterthiophene derivatives exhibiting SmC* phases, with spontaneous polarization exceeding 100 $nCcm^{-2}$ and an effective hole mobility on the order of 10^{-4} $cm^2V^{-1}s^{-1}$. An LC phenylterthiophene derivative bearing a 1,3,3,5,5,7,7-heptamethylcyclotetrasiloxane ring also exhibited an enantiotropic SmC* phase. We observed an anomalous photovoltaic effect based on the coupling of hole transport and ferroelectricity in the SmC* phase.

Anomalous photovoltaic effects are exhibited by semiconductors showing ferroelectricity.[11a] In the presence of internal electric fields formed by spontaneous polarization, excitons generated by illumination dissociate to produce holes and electrons. They are transported to the electrodes by the internal electric field, resulting in photovoltaic effects without the application of any external voltage.

Anomalous photovoltaic effects have been observed in ferroelectric ceramics and their applications in solar cells have been proposed because solar cells can produce higher voltages than their band gaps.[11b-e] However, reports regarding the effects in organic materials have been quite limited. Sasabe and co-workers studied the photovoltaic effect of dye-doped polyvinylidene fluoride, a typical ferroelectric polymer. The density of the dye was very low and the resulting photocurrent was very small.[12a] Tasaka and co-workers observed an anomalous photovoltaic effect in ferroelectric crystals of a triphenylene derivative.[12b] In this study, the sample was composed of vacuum-deposited crystalline thin films.

In addition to conventional ferroelectric LC phases consisting of chiral rod-like molecules, achiral bent-cores[13a] and columnar LC compounds[13b-d] exhibit ferroelectricity in soft mesophases. Ferroelectric switching currents based on polarization inversion and second harmonic generation have been observed. However, anomalous photovoltaic effects have not been confirmed in ferroelectric LC phases.

Experimental Section

Characterization of LC phases

The mesomorphic properties of the phenylterthiophene derivatives were studied by differential scanning calorimetry (DSC), polarizing optical microscopy, and X-ray diffraction (XRD). A polarizing optical microscope (Olympus DP70) equipped with a hand-made hot stage was used for the visual observation of the optical textures. DSC measurements were conducted on a NETZSCH DSC 204 Phoenix. XRD measurements were carried out on a Rigaku Rapid II diffractometer by using Ni-filtered CuKα radiation.

Characterization of carrier transport and spontaneous polarization

Electron mobilities were measured by the time-of-flight (TOF) method.[14] A liquid crystal cell was fabricated by combining two ITO-coated glass plates. The cell was placed on a hot stage and heated at 125 °C. LC samples were melted and filled into the cell via a capillary. The cells were cooled at a rate of 0.1 degree/min. The liquid crystal cell was placed on the hot stage of the TOF setup. DC voltage was applied to the cell using an electrometer (ADC R8252) and a pulse laser was illuminated on the cell. The excitation source was the third harmonic generation of a Nd:YAG laser (Continuum MiniLite II, wavelength = 356 nm, pulse duration = 2 ns) and the induced displacement currents were recorded using a digital oscilloscope (Tektronics TDS 3044B) through a serial resistor. In order to obtain non-dispersive transient photocurrent curves, the penetration depth of the laser light have to be sufficiently thinner than the sample thickness. The penetration depths for three compounds were estimated to be less than 500 nm from the absorption spectra (Fig. S1 in supporting information).

Spontaneous polarization was measured by the triangular wave method. Triangular waves generated by a function generator (NF WF1973) were applied to the LC cells. The induced currents were recorded using a digital oscilloscope (Tektronics TDS 3044B) through a serial resistor.

Synthesis of materials

All the ^{1}H and ^{13}C NMR spectra were recorded on a Varian UNITY INOVA400NB spectrometer. FT-IR measurements were conducted on a JASCO FT/IR-660 Plus spectrometer. 4-Bromo-2-fluorophenol and (S)-2-octanol were purchased from Tokyo Chemical Industry. 5-Bromobithiophene was available from Aldrich-Sigma Inc. 1,1,1,3,3-Pentamethyl-1,3-disiloxane, 1,3,3,5,5,7,7-heptamethyl-1,3,5,7-cyclotetrasiloxane, and the Karstedt catalyst were purchased from Gelest Inc. Tetrahydrofuran, toluene, and dimthoxyethane were obtained from Wako Pure Chemical Industries and were used without purification. Silica gel was purchased from Kanto Chemicals.

LC phenylterthiophene bearing linear alkyl chains exhibit ordered smectic phases at room temperature. Homogenous thin films can be produced by spin-coating and they can be applied in field-effect transistors.[4b] TOF measurements revealed band-like hole transport in the ordered smectic phase.[3h]

Ferroelectric phenylterthiophene derivative **1** bearing a chiral alkyl chain phase was designed. A fluorine atom substituted on the phenyl ring increases spontaneous polarization. Another functional group can be introduced via the double bond at the terminus of the alkyl chain.

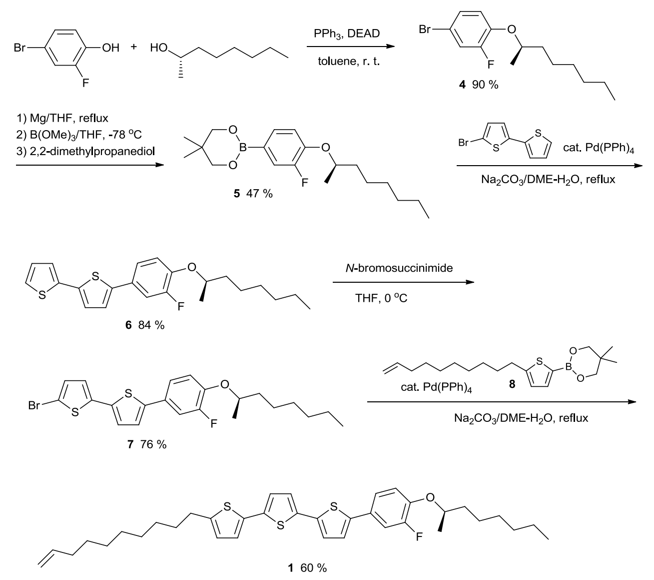

Scheme 1. Synthetic route of ferroelectric phenylterthiophene derivative **1**.

Compound **1** was synthesized as shown in Scheme 1. Phenyl ether **4** was obtained from 4-bromo-2-fluorophenol by the Mitsunobu reaction.[15a] Compound **4** was converted to phenyl boric acid ether **5** via a Grignard reagent. Boric acid **5** was reacted with 5-bromobithiophene via Suzuki coupling[15b] to produce chiral phenylbithiophene derivative **6**. Compound **6** was brominated via reaction with *N*-bromosuccinimide to afford compound **7**, which was coupled with a 2-decenylthienyl boric acid derivative via Suzuki coupling catalyzed by a palladium(0) complex to afford chiral phenylterthiophene derivative **1**.

Conventional liquid crystals bear alkyl side chains of which thermal motion moderately weakens strong intermolecular interaction between aromatic cores. A few liquid crystals bearing oligosiloxane moieties have been investigated.[16] Silsesquioxane derivatives bearing rod-like mesogens exhibit smectic phases.[16a-b] Smectic liquid crystals bearing trisiloxane and disiloxane chains at the ends of their alkyl side chains have been synthesized.[16c-d] They exhibit smectic phases stabilized by the nanosegregation of the oligosiloxane chains. This effect is also seen in bent-core ferroelectric LCs.[16e] Recently, perylene tetracarboxylic bisimide (PTCBI) derivatives bearing oligosiloxane chains that exhibit columnar phases have been reported.[8] PTCBI derivatives bearing tetracyclosiloxane rings also exhibit columnar phases. Nanosegregation of the oligosiloxane moieties is a significant factor in the formation of the columnar phases.[8d]

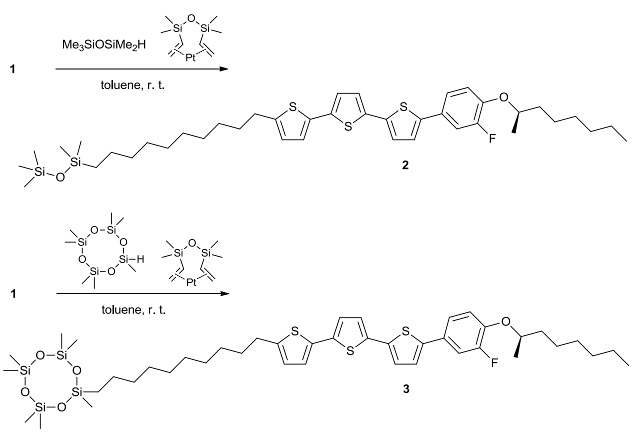

Scheme 2. Synthetic route of chiral phenylterthiophene derivatives bearing oligosiloxane moieties.

In addition to compound **1**, we synthesized chiral phenylterthiophene derivatives **2** and **3** bearing a 1,1,1,3,3-pentamethyl-1,3-disiloxane chain and a 1,3,3,5,5,7,7-heptamethyl-1,3,5,7-cyclotetrasiloxane ring, respectively. The introduction of the oligosiloxane moieties onto the terminus of the alkyl side chains was carried out by hydrosilylation using the Karstedt catalyst,[17] as shown in Scheme 2.

2-(R)-(4-BROMO-2-FLUOROPHENYLOXY)OCTANE (4)

4-Bromo-2-fluorophenol (5.83 g, 30 mmol), (S)-2-octanol (3.90 g, 30 mmol), and triphenylphosphine (7.88 g, 3 mmol) were dissolved in toluene (50 mL). A solution of diethylazodicarboxylate (2.2 mol/L, 15 mL) in toluene was added to the mixture for over 30 min at 0 °C. The solution was stirred at room temperature for 3 h. Then, *n*-hexane (50 mL) was added to the reaction mixture, and the produced white precipitates were filtered. The solvent was evaporated under reduced pressure, and the residual oil was purified by silica gel column chromatography (eluent: *n*-hexane). The pale yellow oil (8.32 g, 27 mmol) was obtained in 90% yield.

^{1}H NMR (400 MHz, $CDCl_3$): δ = 7.21 (dd, 1H, J = 10.8, 2.4 Hz), 7.14 (ddd, 1H, J = 8.8, 2.4, 1.2 Hz), 6.82 (t, 1H, J = 8.8 Hz) , 4.28 (sext, 1H, J = 6.0 Hz), 1.71-1.80 (m, 1H), 1.52-1.60 (m 1H), 1.45-1.21 (m, 8H), 1.27 (3H, d, J = 6.0 Hz), 0.86 (t, 3H, J = 7.2 Hz); IR (ATR): ν = 2927, 2855, 1581, 1491, 1467, 1409, 1378, 1302, 1263, 1206, 1130, 1115, 1035, 973, 939, 854, 800, 724, 638, 573, 452, 401 cm^{-1}; elemental analysis calcd (%) for $C_{14}H_{20}BrFO$: C, 55.46; H, 6.65; Br, 26.35; F, 6.27; O, 5.28; found: C, 55.7; H, 6.7. Exact Mass: 302.07; Molecular Weight: 303.21, m/z: 302.05, 304.05.

4-(2-(R)-OCTYLOXY)-3-FLUOROPHENYLBORIC ACID 2,2-DIMETHYL-1,3-PROPANEDIYL ESTER (5)

Turnings of magnesium (0.84 g, 35 mmol) were dispersed in tetrahydrofuran (30 mL). Compound **4** (7.38 g, 24 mmol) was added to the dispersion and the solvent was gently refluxed. After the formation of the Grignard reagent, the reaction mixture was cooled to -78 °C and a solution (5 mL) of trimethyl borate (2.7 g, 25 mmol) in tetrahydrofuran was added. After stirring the reaction mixture for 3 h, the temperature was increased to room temperature. 2,2-Dimethylpropanediol (3.64 g, 35 mmol) was added to the mixture, which was stirred for 3 h. Water was added to the mixture, and the product was extracted with *n*-hexane. The extract was dried over sodium sulfate. After the solved was evaporated, the residual mixture was purified by silica gel column chromatography (eluent: *n*-hexane/ethyl acetate = 10/1 v/v). Colorless crystals (3.77 g, 11 mmol) were obtained in 45% yield.

^{1}H NMR (400 MHz, $CDCl_3$): δ = 7.47 (d, 1H, J = 2.4 Hz), 7.44 (d, 1H, J = 2.4 Hz), 6.91 (t, 1H, J = 8 Hz), 4.38 (sext, 1H, J = 6 Hz), 3.72 (s 4H), 1.72-1.81 (m, 1H), 1.52-1.61 (m, 1H), 1.35-1.48 (m, 2H), 1.24-1.31 (m, 6H), 1.31 (d, 3H, J = 6.0 Hz), 0.99 (s, 6H), 0.86 (t, 3H, J = 7.2 Hz); IR (ATR): ν = 2958, 2931, 2859, 1612, 1509, 1478, 1424, 1408, 1377, 1339, 1316, 1306, 1267, 1250, 1217, 1195, 1134, 1116, 1038, 991, 937, 892, 853, 813, 775, 748, 726, 703, 692, 675, 642, 564, 537, 496, 453, 401 cm^{-1}; elemental analysis calcd (%) for $C_{19}H_{30}BFO_3$: C, 67.87; H, 8.99; B, 3.22; F, 5.65; O, 14.27; found: C, 67.8; H, 9.1. Exact Mass: 336.23; Molecular Weight: 336.25, m/z: 336.23, 335.23, 337.23, 338.23.

5-{4-(2-(R)-OCTYLOXY)-3-FLUOROPHENYL}BITHIOPHENE (6)

Compound **5** (5.46 g, 16 mmol), 5-bromo-2,2′-bithiophene (4.02 g, 16 mmol), and tetrakistriphenylphosphine palladium(0) (50 mg, 0.043 mmol) were dissolved in dimethoxyethane (150 mL). An aqueous solution of sodium carbonate (10 wt%, 100 mL) was added to the solution, and the resulting reaction mixture was refluxed for 6 h. Dimethoxyethane was removed from the reaction mixture under reduced pressure. The produced precipitates were filtered and purified by silica gel column chromatography (eluent: *n*-hexane/ethyl acetate = 10/1 v/v). Colorless crystals (5.75 g, 15 mmol) were obtained in 90% yield.

^{1}H NMR (400 MHz, $CDCl_3$): δ = 7.30 (dd, 1H, J = 12.0, 2.4 Hz), 7.25 (ddd, 1H, J = 8.8, 2.0, 1.2 Hz), 7.20 (dd, 1H, J = 4.8, 0.8 Hz), 7.17 (dd, 1H, J = 3.6, 1.2 Hz), 7.10 (d, 1H, J = 3.6 Hz), 7.09 (d, 1H, J = 3.6 Hz), 7.01 (dd, 1H, J = 5.6, 3.6 Hz), 6.95 (t, 1H, J = 8.8 Hz) , 4.36 (sextet, 1H, J = 6.0 Hz), 1.83-1.73 (m 1H), 1.64-1.53 (m, 1H), 1.31 (d, 3H, J = 6.0 Hz), 1.30-1.27 (m, 7H), 0.87 (t, 3H, J = 6.8 Hz); IR (ATR): ν = 2951, 2919, 2854, 1611, 1577, 1521, 1504, 1466, 1428, 1375, 1300, 1266, 1245, 1226, 1205, 1123, 1064, 1028, 995, 967, 940, 888, 858, 848, 834, 800, 781, 729, 716, 696, 647, 616, 534, 473, 448, 420 cm^{-1}; Elemental analysis calcd (%) for $C_{22}H_{25}FOS_2$: C, 68.00; H, 6.49; F, 4.89; O, 4.12; S, 16.50; found: C, 68.5; H, 6.8. Exact Mass: 388.13; Molecular Weight: 388.56, m/z: 388.13, 389.14, 390.13, 390.14.

5-BROMO-5′-{4-(2-(R)-OCTYLOXY)-3-FLUOROPHENYL} BITHIOPHENE (7)

Compound **6** (5.75 g, 15 mmol) was dissolved in tetrahydrofuran (200 mL). *N*-bromosucuuinimide (3.2 g, 18 mmol) was added to the solution for over 30 min. After the addition of an aqueous solution of sodium carbonate (10 wt%), the product was extracted with ethyl acetate. The extract was dried over sodium carbonate and the solvent was evaporated under reduced pressure. The residual material was purified by silica gel column chromatography (eluent: *n*-hexane/ethyl acetate = 10/1 v/v). The product was recrystallized from *n*-hexane. Yellow crystals of compound **7** (5.3 g, 11 mmol) were obtained in 76% yield.

^{1}H NMR (400 MHz, $CDCl_3$): δ = 7.28 (dd, 1H, J = 12.0, 2.0 Hz), 7.23 (dd, 1H, J = 8.0, 2.0 Hz), 7.07 (d, 1H, J = 4.0 Hz), 7.03 (d, 1H, J = 4.0 Hz), 6.96 (d, 1H, J = 4.0 Hz) , 6.94 (t, 1H, J = 8.4 Hz), 6.90 (d, 1H, J = 4.0 Hz), 4.36 (sext, 1H, J = 6.0 Hz), 1.73-1.83 (m, 1H), 1.56-1.63 (m, 1H), 1.35-1.51 (m, 2H), 1.31, (d, 3H, J = 6.0 Hz), 1.23-1.35 (m, 6H), 0.86 (t, 3H, J = 6.8 Hz); IR (ATR): ν = 2927, 2855, 1615, 1575, 1556, 1524, 1498, 1460, 1427, 1377, 1350, 1299, 1268, 1238, 1174, 1126, 1057, 999, 969, 937, 864, 788, 724, 688, 610, 577, 532, 477, 448 cm^{-1}; Elemental analysis calcd (%) for $C_{22}H_{24}BrFOS_2$: C, 56.53; H, 5.17; Br, 17.09; F, 4.06; O, 3.42; S, 13.72; found: C, 56.8; H, 5.1. Exact Mass: 466.04; Molecular Weight: 467.46, m/z: 468.04, 466.04, 469.04.

2-(9-DECENYL)THIENYLBORIC ACID 2,2-DIMETHYL-1,3-PROPANEDIYL ESTER (8)

Reagent 2-(9-decenyl)thiophene (30.0 g, 0.13 mol) was dissolved in tetrahydrofuran (20 mL). The solution was cooled to 0 °C and *n*-butyllithium (99.7 mL, 1.6 M/*n*-hexane solution) was added over 2 h. The reaction mixture was cooled to -78 °C and a solution (20 mL) of trimethyl borate (13.8 g, 0.13 mol) in tetrahydrofuran was added. While stirring the reaction mixture for 6 h, the temperature of the reaction mixture increased to room temperature. To the mixture, 2,2-dimethyl-1,3-propanediol (13.8 g, 0.13 mol) was added. After 4 h, water was added to the mixture. The product was extracted with ethyl acetate and the extract was dried over sodium sulfate. The crude product was purified by silica gel chromatography (eluent: *n*-hexane). The white solid (20.4 g, 60 mmol) was obtained in 45% yield.

^{1}H NMR (400 MHz, $CDCl_3$): δ = 7.38 (d, 1H, J = 4.0 Hz), 6.81 (d, 1H, J = 4.0 Hz), 5.77 (ddt, 1H, J = 16.8, 10.4, 6.4 Hz), 4.96 (dd, 1H, J = 16.8, 3.6 Hz), 4.88 (dd, 1H, J = 10.4, 3.6 Hz) , 3.73 (s, 4H), 2.80 (t, 2H, J = 8.0 Hz), 2.02 (quartet, 2H, J = 6.4 Hz), 1.68 (quintet, 2H, J = 8.0 Hz), 1.24-1.39 (m, 10H), 1.00 (s, 6H); IR (ATR): ν = 2924, 2850, 1643, 1537, 1480, 1465, 1434, 1415, 1378, 1326, 1286, 1252, 1206, 1108, 1043, 993, 905, 848, 811, 779, 722, 696, 680, 658, 571, 497, 483 cm^{-1}; Elemental analysis calcd (%) for $C_{19}H_{31}BO_2S$: C, 68.26; H, 9.35; B, 3.23; O, 9.57; S, 9.59; found: C, 68.4; H, 9.4. Exact Mass: 334.21; Molecular Weight: 334.32, m/z: 334.21.

5-(9-DECENYL)-5″-{4-(2-(R)-OCTYLOXY)}-3-FLUOROPHENYL} -2,2′-5′,2″-TERTHIOPHENE (1)

Compound **7** (2.7 g, 5.8 mmol), compound **8** (2.89 g, 8.7 mmol), and tetrakistriphenylphosphine palladium(0) (50 mg, 0.043 mmol) were dissolved in diethoxyethane (150 mL). An aqueous solution of sodium carbonate (10 wt%, 100 mL) was added, and the mixture was refluxed for 6 h. Dimethoxyethane was removed from the reaction mixture under reduced pressure. The produced precipitate was filtered and purified by silica gel column chromatography (eluent: *n*-hexane/ethyl acetate = 10/1 v/v). Pale yellow crystals (1.56 g, 2.6 mmol) were obtained in 44% yield.

^{1}H NMR (400 MHz, $CDCl_3$): δ = 7.29 (dd, 1H, J = 12.0, 2.4 Hz), 7.25 (ddd, 1H, J = 8.4, 2.0, 1.2 Hz), 7.09 (d, 1H, J = 3.6 Hz), 7.07 (d, 1H, J = 3.6 Hz), 7.04 (d, 1H, J = 4.0 Hz), 6.98 (d, 1H, J = 3.6 Hz, 6.97 (d, 1H, J = 3.6 Hz), 6.94 (t, 1H, J = 6.3 Hz), 6.67 (d, 1H, J = 3.6 Hz), 5.80 (ddt, 1H, J = 16.8, 10.4, 6.8 Hz), 5.00 (ddd, 1H, J = 16.8, 3.6, 1.2 Hz), 4.92 (ddt, 1H, J = 10.4, 3.6, 1.2 Hz), 4.36 (sextet, 1H, J = 6.0 Hz), 2.78 (2H, t = J = 7.6 Hz), 2.03 (quintet, 2H, J = 6.8 Hz), 1.82-1.73 (m, 1H), 1.67 (quintet, 2H, J = 7.2 Hz), 1.64-1.56 (m, 1H), 1.40-1.25 (m, 18H), 1.31 (d, 3H, J = 6.4 Hz), 0.87 (t, 3H, J = 6.4 Hz); ^{13}C NMR (100 MHz $CDCl_3$): δ = 145.9, 139.4, 137.0, 136.4, 135.6, 134.6, 125.0, 124.5, 124.3, 123.7, 123.6, 121.6, 121.5, 118.0, 114.3, 114.0, 113.8, 113.5, 76.8, 36.7, 34.0, 32.0, 31.8, 30.4, 29.6, 29.5, 29.4, 29.3, 29.2, 29.1, 25.6, 22.8, 20.0, 14.3, 14.2; IR (ATR): ν = 3072, 2919, 2848, 1640, 1616, 1576, 1546, 1524, 1506, 1464, 1427, 1379, 1303, 1268, 1234, 1209, 1123, 1069, 996, 942, 911, 894, 857, 810, 799, 790, 726, 661, 630, 594, 549, 474, 447 cm^{-1}; Elemental analysis calcd (%) for $C_{36}H_{45}FOS_3$: C, 71.01; H, 7.45; F, 3.12; O, 2.63; S, 15.80; found: C, 71.4; H, 7.6. Exact Mass: 608.26; Molecular Weight: 608.94, m/z: 608.26, 609.27.

5-{10-(1,1,1,3,3-PENTAMETHYL-1,3-DISILOXANYL)DECAN-1-YL}-5″-{4-(2-(R)-OCTYLOXY)}-3-FLUOROPHENYL}-2,2′-5′,2″-TERTHIOPHENE (2)

Compound **1** (0.50 g, 0.82 mmol) and 1,1,1,3,3-pentamethyl-1,3-disiloxane was dissolved in toluene (30 mL). The Karstedt catalyst (1,3-divinyl-1,1,3,3-tetramethyldisiloxane platinum(0), 10 μL, 3.4 atom% in xylene) was added, and the solution was stirred for 12 h at room temperature. The solvent was evaporated and the resulting crude product was purified by silica gel column chromatography (eluent: *n*-hexane/ethyl acetate = 10/1 v/v). The yellow waxy product (0.21 g, 0.27 mmol) was obtained in 34% yield.

^{1}H NMR (400 MHz, $CDCl_3$): δ = 7.30 (dd, 1H, J = 12.0, 2.0 Hz), 7.25 (dd, 1H, J = 8.4, 2.0 Hz), 7.10 (d, 1H, J = 4.0 Hz), 7.08 (d, 1H, J = 4.0 Hz), 7.05 (d, 1H, J = 4.0 Hz), 6.99 (d, 1H, J

= 3.6 Hz), 6.97 (d, 1H, J = 3.6 Hz), 6.95 (t, 1H, J = 6.3 Hz), 6.67 (d, 1H, J = 3.6 Hz), 4.36 (sextet, 1H, J = 6.0 Hz), 2.78 (t, 2H, J = 3.6 Hz), 1.84-1.75 (s, 1H), 1.69 (quint, 2H, J = 7.2 Hz), 1.65-1.57 (m, 1H), 1.42-1.25 (m, 18H), 1.32 (d, 3H, J = 6.4 Hz), 0.87 (t, 3H, J = 6.8 Hz), 0.49 (t, 2H, J = 7.2 Hz), 0.05 (s, 9H), 0.02 (6H, s); ^{13}C NMR (100 MHz $CDCl_3$): δ = 0.6, 2.2, 14.3, 18.6, 20.0, 22.8, 23.5, 25.6, 29.3, 29.4, 29.6, 29.8, 30.4, 31.8, 32.0, 33.6, 36.7, 76.8, 113.8, 114.0, 118.0, 121.5, 121.6, 122.5, 123.6, 123.7, 124.3, 124.5, 125.0, 134.6, 135.6, 136.5, 137.1, 145.9; IR (ATR): ν = 2957, 2922, 2853, 1575, 1545, 1523, 1505, 1445, 1378, 1300, 1252, 1233, 1125, 1052, 942, 840, 789, 753, 625, 477, 447 cm^{-1}; Elemental analysis calcd (%) for $C_{41}H_{61}FO_2S_3Si_2$: C, 65.03; H, 8.12; F, 2.51; O, 4.23; S, 12.70; Si, 7.42; found: C, 65.40; H, 8.1. Exact Mass: 756.34; Molecular Weight: 757.29, m/z: 756.34, 757.34, 758.33, 758.34, 759.33.

5-{10-(1,3,3,5,5,7,7-HEPTAMETHYL-1,3,5,7-CYCLOTETRASILOXAN-1-YL)DECAN-1-YL}-5″-{4-(2-(R)-OCTYLOXY)}-3-FLUOROPHENYL}-2,2′-5′,2″-TERTHIOPHENE (3)

Compound **1** (0.75 g, 1.24 mmol) and 1,3,3,5,5,7,7-heptamethyl-1,3,5,7-cyclotetrasiloxane (0.52 g, 1.86 mmol) were dissolved in toluene (30 mL). The Karstedt catalyst (1,3-divinyl-1,1,3,3-tetramethyldisiloxane platinum(0), 10 μL, 3.4 at% in xylene) was added, and the solution was stirred for 12 h at room temperature. The solvent was evaporated and the resulting crude product was purified by silica gel column chromatography (eluent: *n*-hexane/ethyl acetate = 10/1 v/v). The yellow waxy product (0.21 g, 0.27 mmol) was obtained in 34% yield.

^{1}H NMR (400 MHz, $CDCl_3$): δ = 7.31 (dd, 1H, J = 12.4, 2.4 Hz), 7.26 (ddd, 1H, J = 8.4, 2.4, 1.2 Hz), 7.10 (d, 1H, J = 3.6 Hz), 7.09 (d, 1H, J = 3.6 Hz), 7.06 (d, 1H, J = 4.0 Hz), 7.00 (d, 1H, J = 4.0 Hz), 6.98 (d, 1H, J = 4.0 Hz), 6.96 (t, 1H, J = 8.4 Hz) , 6.68 (d, 1H, J = 4.0 Hz), 4.37 (sextet, 1H, J = 6.0 Hz), 2.79 (t, 2H, J = 3.6 Hz), 1.84-1.75 m, 1H), 1.68 (quintet, 2H, J = 7.2 Hz), 1.65-1.57 (m. 1H), 1.42-1.25 (m, 18H), 1.33 (d, 3H, J = 6.8 Hz), 0.89 (t, 3H, J = 6.8 Hz), 0.50 (dd, 2H, J = 9.2, 6.0 Hz), 0.09 (s, 18H), 0.07 (s, 3H); ^{13}C NMR (100 MHz $CDCl_3$): δ = 145.9, 136.4, 135.5, 135.4, 134.6, 125.0, 124.5, 124.3, 123.7, 123.6, 121.6, 121.5, 118.0, 117.9, 114.0, 113.8, 113.7, 76.7, 36.6, 33.3, 33.2, 31.9, 31.8, 30.4, 30.3, 29.8, 29.7, 29.5, 29.4, 29.3, 25.6, 25.5, 23.1, 22.8, 20.0, 17.3, 14.2, 0.96, 0.93; IR (ATR): ν = 2961, 2923, 2853, 1545, 1524, 1507, 1445, 1378, 1300, 1259, 1234, 1060, 941, 854, 789, 696, 553, 477 cm^{-1}; Elemental analysis calcd (%) for $C_{43}H_{67}FO_5S_3Si_4$: C, 57.93; H, 7.57; F, 2.13; O, 8.97; S, 10.79; Si, 12.60; found: C, 57.8; H, 7.6. Exact Mass: 890.32; Molecular Weight: 891.52, m/z: 890.52, 891.52, 892.52.

Results and Discussion

Characterization of mesophases of compounds 1-3

Compounds **1-3** exhibited an enantiotropic SmC* phase as well as a more ordered smectic G (SmG) phase. Figure 1 shows the DSC thermograms of compounds **1-3**. Compound **1** formed crystals via recrystallization from *n*-hexane. The crystals changed to the SmG phase at 58 °C. Upon cooling, they did not crystallize and the SmG phase was retained. Compounds **2-3** formed waxy mesomorphic precipitates during recrystallization from *n*-hexane and did not crystallize upon cooling to -100 °C. Compounds **1** and **2** exhibited an SmC* phase between 124 and 140 °C and between 116 and 129 °C, respectively. The SmG phases were observed below the SmC* phase. As reported previously for the LC molecules bearing disiloxane chains at the end of their alkyl side chain,[16c-e] the temperature range of the SmC* phase for compound **2** was slightly lower than that of compound **1**.

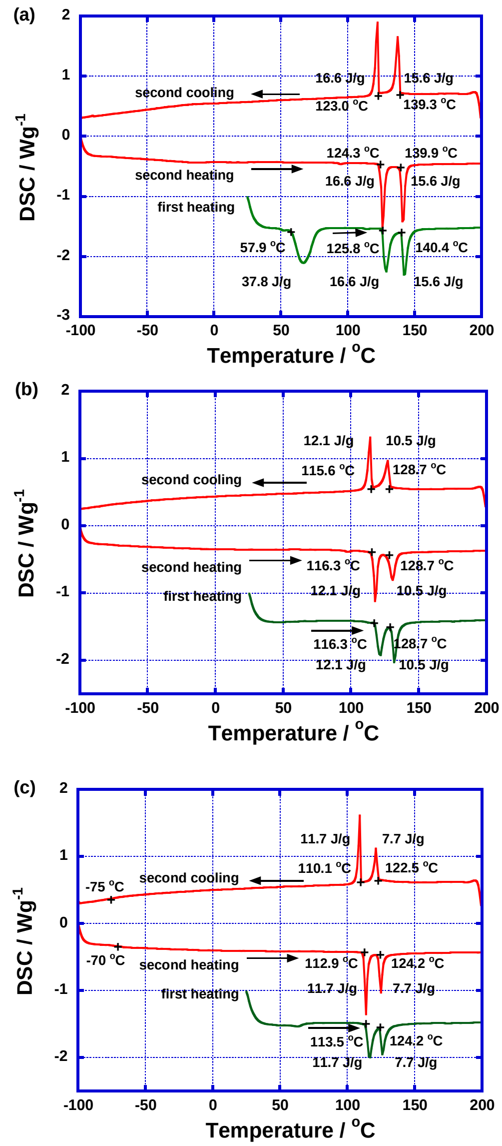

Figure 1. DSC thermograms of (a) compound **1**, (b) compound **2**, and (c) compound **3**. The heating and cooling rates are 10 K/min. The green curves exhibit the thermograms of materials formed via recrystallization from *n*-hexane.

Surprisingly, compound **3** with a bulky cyclotetrasiloxane ring also exhibited a SmC* phase between 110 and 122 °C. Below 110 °C, a SmG phase appeared and a glass transition associated with the thermal motion of the cyclotetrasiloxane moiety was observed at – 70 °C.

Figure 2(a) shows the XRD patterns of compound **1**. In the high-temperature phase, peaks derived from the (001), (002), and (003) diffraction planes were observed at $2\theta = 2.97°$, 6.35°, and 9.47° in the low-angle region. A broad halo associated with the liquid-like packing of the alkyl chains appeared around $2\theta = 16°$. The layer spacing estimated from the (001) diffraction was 29.6 Å, which was shorter than the extended molecular length of 37 Å. Therefore, this phase was assigned to the SmC* phase. In the low-temperature phase, wide-angle peaks derived from the (200), (010), (110), and (210) diffraction planes were observed, indicating a long-range rectangular order of the molecular position within the layers. The layer spacing was shorter than the extended molecular length, indicating that the low-temperature phase was an SmG phase.[18]

Figure 2(b) displays the XRD patterns of compound **2**. In the high-temperature phase, the ratio of the lattice constants determined by the low angle peaks at $2\theta = 2.61°$, 4.04°, 4.83°, and 9.23° was 1/2:1/3:1/4:1/7. This result suggested dimeric aggregation in the low-temperature phase, and these peaks were indexed to the (002), (003), (004), and (007) diffraction planes. The diffraction peak derived from the (001) plane was not observed because it was shielded by a stopper. In the wide-angle region, two halos around 12° and 18° were attributed to the liquid-like orders of disiloxane and the alkyl chains, respectively. The lattice constant derived from the (002) diffraction was 33.5 Å, which was shorter than the fully extended length of compound **2** (42 Å), indicating that the LC molecules tilt from the normal of the layers or the disiloxane chains interdigitate. Thus, the high-temperature phase was identified as the SmC* phase. In the low-temperature phase, a broad peak around 18° was observed in addition to the low-angle peaks associated with the lamellar organization of the LC molecules. This broad peak suggested a hexatic bond order within the layers. The low-temperature phase should be a smectic F phase. From the low-angle peaks, the dimeric structure was retained in the low-temperature phase. The interaction between the disiloxane chains promoted the formation of the dimeric layer structure.

Figure 3(c) shows the XRD patterns of compound **3** bearing a bulky cyclotetrasiloxane ring. In the high-temperature phase, three low angle peaks derived from the (001), (002), (003), and (004) diffraction planes were observed. In the high-angle region, two halos appeared. The halo around 18° was attributed to the liquid-like packing of alkyl chains, and the other halo around 12° was ascribed to the disordered aggregation of cyclotetrasiloxane rings. No diffraction peaks indicating the long-range order of the molecular position within the smectic layers were observed. The layer spacing of 36.2 Å was shorter than the extended molecular length, indicating a tilted orientation of the molecules in the smectic layers. Therefore the high-temperature phase was assigned to the SmC* phase.

The XRD patterns revealed that the low-temperature phase should be an SmF phase. Low-angle peaks were assigned to the (001), (002), (003), and (004) diffraction planes. Similar to compound **2**, the positional order within the smectic layers was ambiguous in the low-temperature phase. The layer spacing was also shorter than the extended molecular length. Two broad halos were observed around 12º and 18º, derived from the liquid-like aggregation of the cyclotetrasiloxane rings and alkyl chains, respectively. Compared to the SmG phase of compound **1**, diffraction peaks associated with the positional order within the smectic layers were broad, indicating a more disordered structure in the SmF phase[18] for compound **3**.

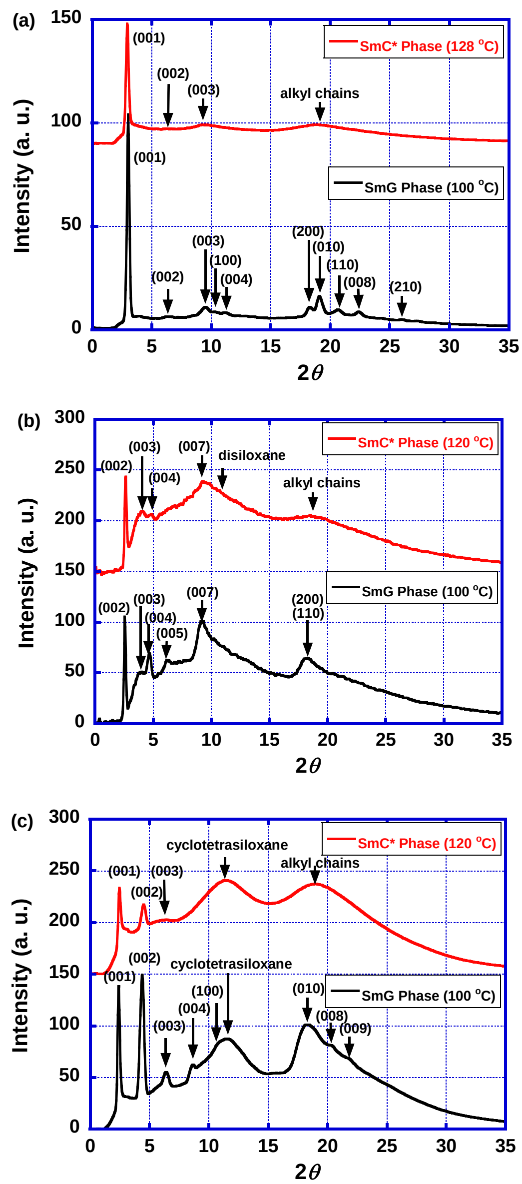

Figure 2. X-ray diffraction patterns of compound **1** in the (a) SmC* phase at 128 °C and (b) SmG phase at 100 °C.

In contrast to compounds **1** and **3**, compound **2** exhibited a dimeric SmC* phase. In compound **2**, the interaction between the disiloxane chains and their interdigitation should promote the formation of a dimeric layer structure. In compound **3**, the same interaction between the cyclotetrasiloxane rings should be plausible. However, the interdigitation between the cyclotetrasiloxane rings of compound **3** is difficult because of their bulkiness as compared to the disiloxane rings of compound **2**. Therefore, a monomeric layer structure should be favorable in compound **3** in spite of the presence of oligosiloxane moieties.

Polarizing optical micrographic textures of compounds 1-3

In the SmC* phases of compounds **1** and **3**, broken fan-like domains with stripe patterns were observed without an electric field under a polarizing optical microscope (Figure 4). The stripe patterns were derived from the helical structures of the SmC* phases of the compounds. The helical pitches were about 2 μm for compound **1**, 3 μm for compound **2**, and 10 μm for compound **3**.

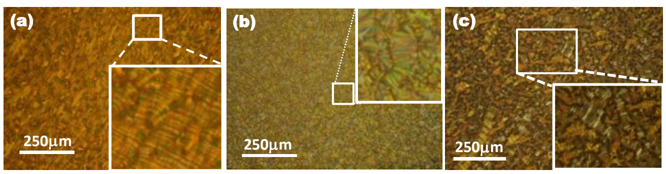

Figure 4. Polarizing optical micrographs without application of a DC bias in the SmC* phase of (a) compound **1** at 130 °C and (b) compound **3** at 120 °C.

As observed in the conventional ferroelectric SmC* phases, the stripe patterns disappeared when a DC voltage was applied to the LC cells. As shown in Figure 5, the transmittances of the domains changed with the crossed polarizers when the polarity of the DC voltage was inverted. This behavior is typical of a ferroelectric SmC* phase. The transmittance switching of the optical textures was based on the change of the molecular orientation caused by the inversion of the spontaneous polarization.

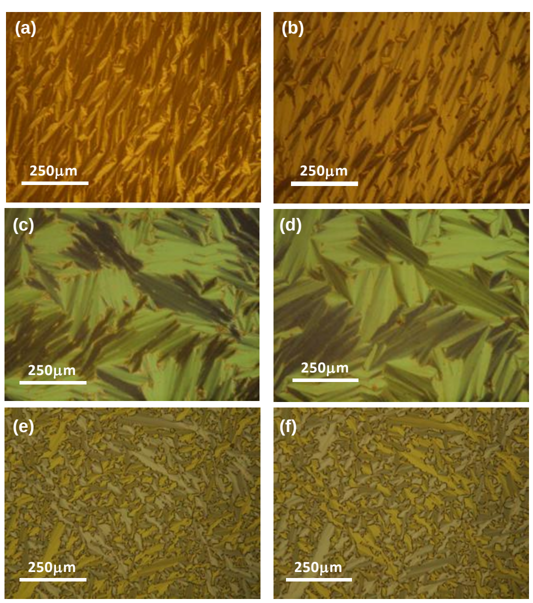

Figure 5. Polarizing optical micrographs of the SmC* phases for compound **1** under the application of a (a) positive and (b) negative bias (±1.5 V for 4-μm thick sample) as well as for compound **2** ((c) positive and (d) negative bias (±5 V for 9-μm thick sample)) and compound **3** ((e) positive and (f) negative bias (±5 V for 9-μm thick sample)).

Characterization of the spontaneous polarization in the SmC* phases of compounds 1-3

Spontaneous polarizations in the SmC* phases of compounds **1-3** were determined by the triangular wave method. Figure 6(a) shows the polarization inversion current curves in the SmC* phases of compounds **1-3** when triangular voltages were applied to the LC cells. As observed in the SmC* phase of conventional ferroelectric LCs, current peaks caused by polarization inversion were obtained in the current response curves.

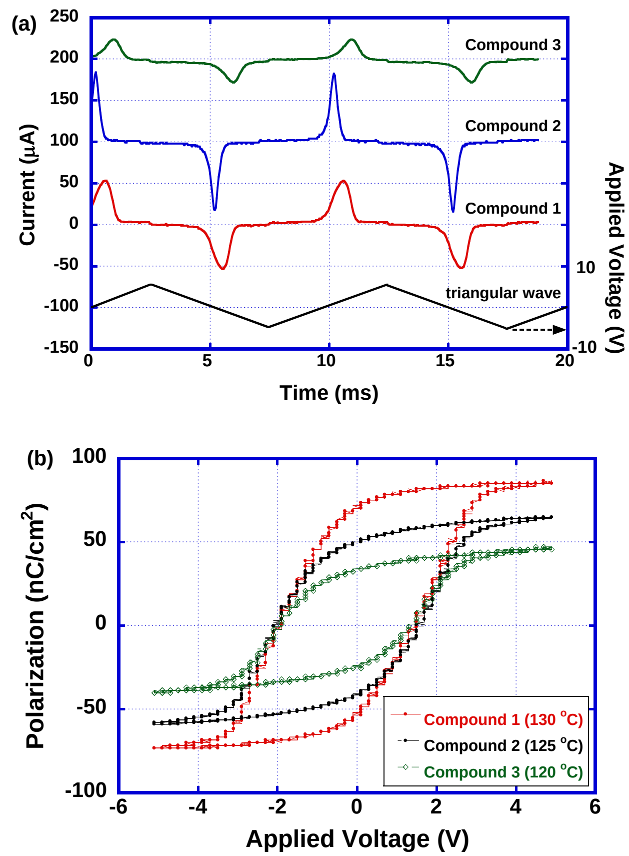

Figure 6. Polarization inversion current measured by the triangular wave method in the SmC* phase of compound **1** at 130 °C, compound **2** at 125 °C, and compound **3** at 120 °C. The sample thickness was 2 μm. (b) Hysteresis loops in the SmC* phase of compounds **1** (130 °C), **2** (125 °C), and **3** (120 °C). The frequency was 100 Hz and the capacitance of serial capacitance was 33 nF.

In the SmC* phase of compound **1**, the polarization inversion occurred in several microseconds. This rate was slower than that of conventional ferroelectric LCs. The higher viscosity attributed to strong π-π interactions in the SmC* phase of compound **1** should result in this slow inversion. The spontaneous polarization was determined to be 151 $nCcm^{-2}$. This value was much higher than those of classical ferroelectric LCs such as DOBANBC[9b] and ferroelectric phenylnaphthalene derivatives.[10]

In the SmC* phase of compound **2**, the spontaneous polarization was 120 $nCcm^{-2}$. The bulky disiloxane moiety should slightly inhibit closed molecular aggregation in the

SmC* phase of compound **2** and decrease the macroscopic polarization. This more disordered structure of the SmC* phase of compound **2** than that of compound **1** should decrease the viscosity of the SmC* phase of compound **2**. The polarization inversion was more rapid than that of compound **1**.

In the SmC* phase of compound **3**, the disorder of the molecular aggregation structure is more remarkable, compared to those of compared to compounds **1** and **2**. The measurement revealed a spontaneous polarization of 62 $nCcm^{-2}$ in the SmC* phase of compound **3**. This value was lower than that of compound **1** by a factor of 2.5. Compound **3** bears a very bulky cyclotetrasiloxane ring which perturbs closed molecular aggregation in its SmC* phase. This disordered structure inhibits macroscopic ordering of molecular dipole moments. The response time in the SmC* phase of compound **3** was two times slower than that of compound **1**. This slower response in the polarization current for compound **3** should also be attributed to the higher viscosity in its SmC* phase. The temperature range of the SmC* phase of compound **3** was 10 degrees lower than that of compound **1** and thermal fluctuation is smaller in the SmC* phase of compound **3** than the case of compound **1**. Larger molecular weight of compound **3** than that of compound **1** should also contribute to the higher viscosity in the SmC* phase of compound **3**.

Figure 6(b) exhibits hysteresis D-V loops in the SmC* phase of compounds **1-3** measured by a Sawyer-Tower method. For the SmC* phase of all the compounds, ferroelectric hysteresis loops were obtained. The values of the obtained spontaneous polarizations for compounds **1-3** were 83 $nCcm^{-2}$, 58 $nCcm^{-2}$, and 38 $nCcm^{-2}$. They are about half of those determined by the triangular method. The hysteresis loop indicates that the coercive voltage and electric field in the SmC* phase of compound **1** are around 1 V and 5×10^{3} Vcm^{-1}, respectively.

Carrier transport properties in the SmC* phase of compounds 1-3

The carrier mobilities in the SmC* phases of compounds **1-3** were determined by the TOF method. In the SmC* phases of compounds **1-3**, non-dispersive transient photocurrent signals originating from hole transport were observed. The transient photocurrent signals for electrons were too weak for the electron mobilities to be determined.

Figure 7 (a) shows the transient photocurrent curves for holes in the SmC* phase of compound **1** at 130 °C. Non-dispersive transient photocurrent curves with initial spikes were obtained and transit times were determined by the linear plots of the curves. The hole mobility calculated from the transit times was 3×10^{-4} $cm^2V^{-1}s^{-1}$, and was independent of the electric field and temperature.

Figure 7(b) shows the transient photocurrent curves for holes in the SmC* phase of compound **2** at 125 °C. Non-dispersive transient curves were obtained and the hole mobility was determined to be 2×10^{-4} $cm^2V^{-1}s^{-1}$. The hole mobility was independent of the electric field and temperature in the SmC* phase.

Figure 7 (c) shows the transient photocurrent curves for the holes in the SmC* phase of compound **3** at 120 °C. Non-dispersive transient photocurrent curves with delays in the rising of the curves were observed. The transit times were determined in the linear plots of the transient photocurrent curves. The hole mobility was 1×10^{-4} $cm^2V^{-1}s^{-1}$. The hole mobility was also independent of the electric field and temperature.

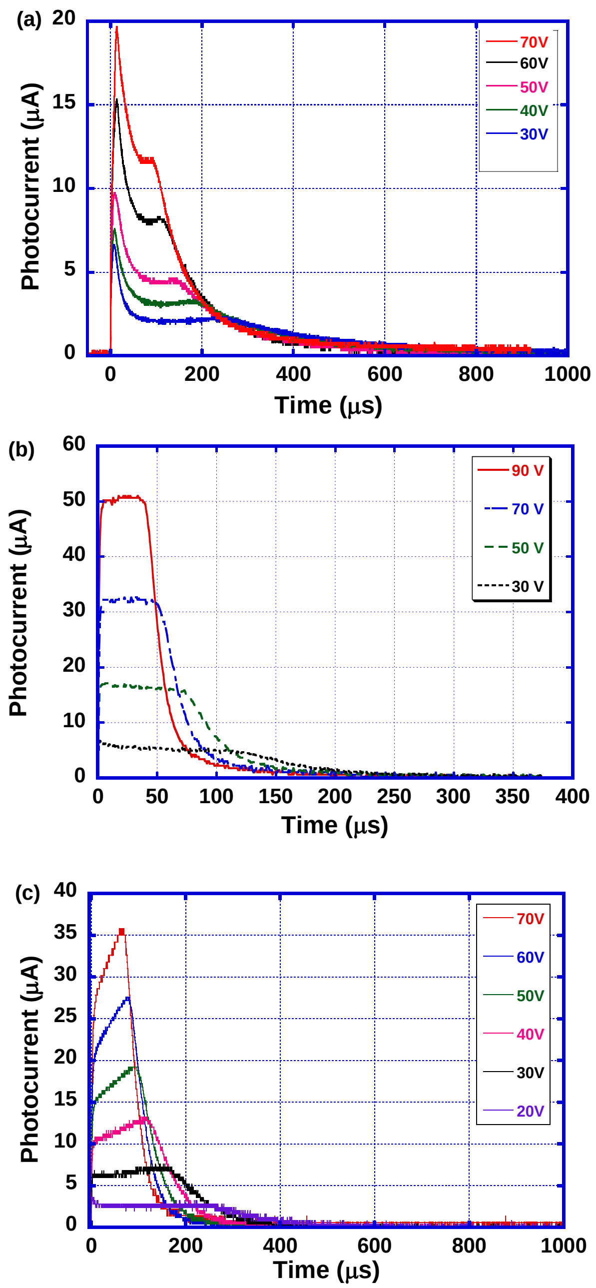

Figure 7. Transient photocurrent curves for holes in the SmC* phases of (a) compound **1** at 130 °C (sample thickness = 15 μm), (b) compound **2** at 125 °C (sample thickness = 9 μm), and (c) compound **3** at 120 °C (sample thickness = 9 μm).

In the smectic phases of LC semiconductors above room temperature, temperature- and field-independent mobilities are typically observed.[2a,b] These temperature- and field-independent mobilities are explained based on Gaussian disorder[19] or small polaron hopping models.[20] In contrast to amorphous organic semiconductors in which carrier mobilites are strongly dependent on the electric field and the temperature, smaller energetic and positional disorders result in a smaller dependency of the carrier mobilities in the liquid crystal phases.[2g,3g] In addition, the positive temperature-dependence of the carrier mobility is cancelled by the negative temperature-dependence derived from the thermal fluctuation of the mesomorphic structures.[8e]

In amorphous organic semiconductors, the dipole moments of semiconductor molecules increase the energetic disorder because local electric fields produced by randomly oriented molecular dipoles increase the dispersion width of the energy levels of semiconductor molecules.[21] In a columnar phase of a nitrotriphenylene derivative, increased energetic disorder was reported.[21c] However, molecular dipoles are oriented in one direction in the SmC* phase under the application of electric fields. Therefore, temperature- and field-dependencies in the SmC phases of compounds **1** and **3** should not be remarkable.

Anomalous photovoltaic effect in the SmC* phase of compounds 1 and 3

Conventional photovoltaic effects are caused by an internal electric field produced at the p-n junction or Schottky barrier formed at the interface between a semiconductor layer and an electrode. In contrast, anomalous photovoltaic effects are observed in ferroelectrics and originate from an electric field generated by spontaneous polarization. The polarity of the photovoltaic effect is determined by the polarity of the internal electric field. After the application of a DC voltage pulse, light illumination under zero bias produces a photocurrent with a reversed polarity to the DC bias prior to the light illumination. The inversion of the DC bias direction changes the polarity of the photovoltaic effect under zero bias.[12b]

Figure 8(a) shows the steady state photocurrent response under zero bias. In the initial state in which the sample was cooled from the isotropic phase to the SmC* phase, the photocurrent response was quite ambiguous. In this state, the dipole moments of the molecules did not orient macroscopically because of the helical structure of the SmC* phase. However, after the application of the DC voltage, clear photocurrent response was observed. It should be emphasized that the polarities of the photocurrents were opposite to those of the DC biases applied prior to light illuminations. In these states after the application of the positive and negative biases, the helical structures disappeared and macroscopic spontaneous polarizations and internal electric fields were produces. The internal fields are opposite to the polarities of the DC biases applied prior to the light illumination.

When the illuminated electrode was biased negatively, the photocurrent response under zero bias was stronger than that observed after the application of the positive DC voltage. In the case of the stronger photocurrent response, the photocurrent was attributed to the hole transport. Compared to the electrons, the holes are generated and transported efficiently in the SmC* phase as verified in the TOF experiments.

Figure 8(b) exhibits the current-voltage characteristic of the same sample of compound **1**. The open circuit voltage was 0.35 V and short circuit current was 200 nA. In the SmC* phase of compound **1**, the coercive electric field and voltage are 1×10^4 Vcm^{-1} and 2 V at 100 Hz, respectively, as shown in Figure 6(b). This result indicates that the spontaneous polarization is retained for several ms. However, the spontaneous polarization should be partially relaxed on the time scale (several second) of the experiment of the steady-state photocurrent measurement.

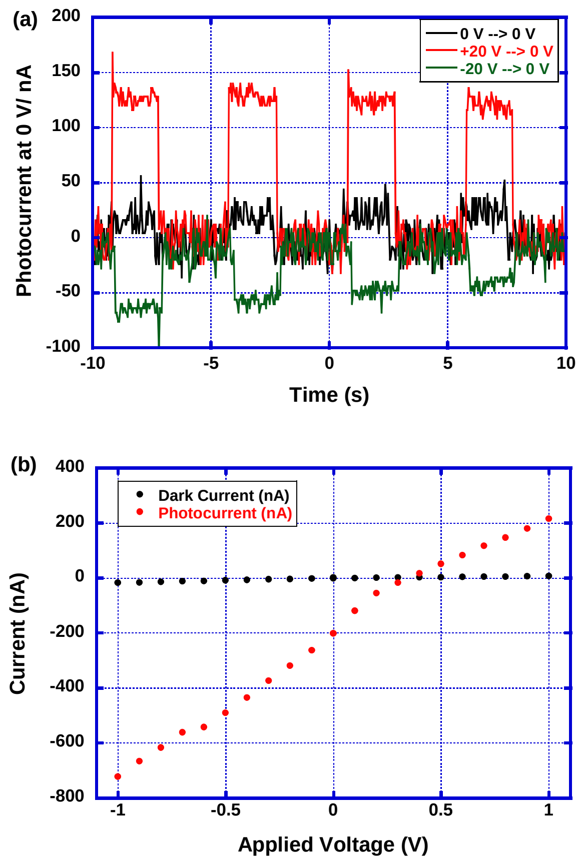

Figure 8 (a) Steady state photocurrent response in the SmC* phase of compound **1** at 127 °C under the zero bias. The sample thickness was 2 μm and the electrode area was 0.16 cm^2. (b) Current-voltage characteristics in the same sample. The wavelength and intensity of the illuminated light were 360 nm and 3 mW/cm^2, respectively.

Transient photovoltaic effect was also studied. Figure 9 (a) shows the photocurrents under zero bias after pulse laser illumination in the SmC* phase of compound **1** at 130 °C. Prior to the photocurrent measurement, DC biases of 0 V, +20 V, and -20 V were applied to the sample for 1 min. When the DC bias was 0 V prior to illumination, the photocurrent under zero bias was almost zero. Immediately after the light illumination, a non-zero photocurrent was generated, but it was very low. A strong spike should be caused by the local electric field formed on the electrode surface, due to local molecular alignment. When the DC bias was +20 V prior to the light illumination, a photocurrent of approximately 10 nA was generated. The polarity of the photocurrent was reversed to that of the DC bias prior to the illumination. In the case of the DC bias of -20 V before the illumination, a photocurrent of over 10 nA was generated and the polarity was reversed. In the isotropic phase, the generated photocurrents under zero bias were much smaller than those in the SmC* phase. In the SmG phase, a non-zero photocurrent was observed, but such a change in the photocurrent polarity did not occur.

Figure 9(b) shows the photocurrent curves in the SmC* phase of compound **1** at 130 °C under the DC bias of +0.5 and -0.5 V, which corresponds to the electric field of $\pm 2.5\times10^{3}$ Vcm^{-1}. In the electric field region, the diffusion of the charge carrier was dominant over the drift movement of the carriers resulting in a featureless current decay without clear kink points.

The strengths and shapes of the transient photocurrents were similar to those of the zero-field photocurrents after DC bias application shown in Figure 9(a). This indicated that an internal electric field on the order of 10^{3} Vcm^{-1} was formed by spontaneous polarization in the ferroelectric SmC* phase.

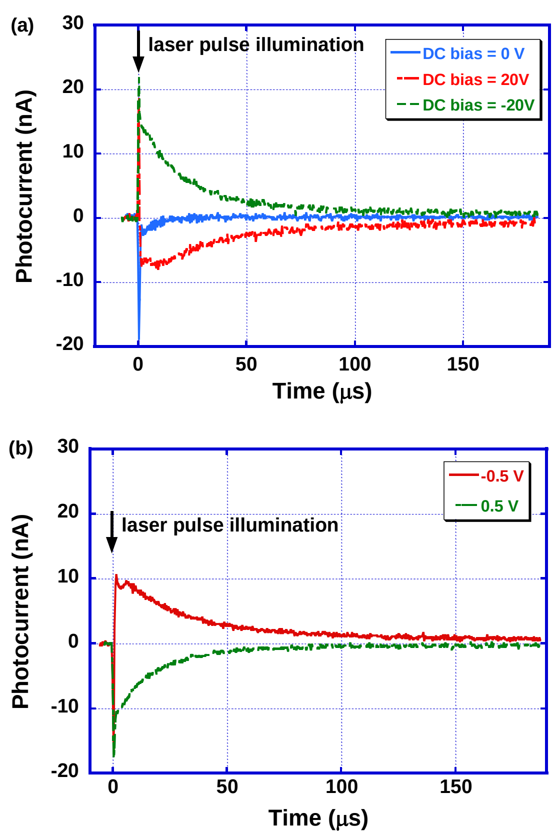

Figure 9. (a) Photocurrent under zero bias after laser pulse (wavelength = 356 nm, pulse duration = 2 ns) illumination in the SmC* phase of compound **1** at 130 °C. Before the laser illumination, DC voltages of 0, 20, and -20 V were applied to the sample (thickness of 2 μm) for 1 min. (b) Transient photocurrent curves under DC biases of 0.5 and -0.5 V in the SmC* phase of compound **1**.

The estimated value of the internal electric field was on the same order of that determined by the steady-state photocurrent measurement as shown in Figure 8(b). These internal electric field values determined by the steady and transient photocurrent measurements were smaller than the coercive electric field determined at 100 Hz by the Sawyer-Tower method, as shown in Figure 6(b). The partial relaxation of the spontaneous polarization should decrease the internal electric field.

The value of spontaneous polarization (145 $nCcm^{-2}$) should lead to the production of an electric field on the order of 5×10^{5} Vcm^{-1}. In this experiment, the induced internal field was on the order of 10^{3} Vcm^{-1}, which was much smaller than the theoretically expected value. In this case, the sample thickness was 2 μm. Near the electrode-LC interface, ferroelectric polarization should be retained although it should be relaxed in the bulk under the zero-field because of reconstruction of the helical structure.

This zero-field photocurrent was not observed in the isotropic phase without spontaneous polarization. In the SmG phase, the inversion of the sign of the zero-field photocurrent did not occur when the polarity of the DC voltage was changed prior to the laser illumination.

For compounds **2** and **3**, a zero-field photocurrents were observed in the SmC* phase and the polarities were changed according to the sign of the DC bias prior to laser illumination. However, the value of the photocurrent was weaker than that of compound **1**. Such photovoltaic effects can be caused by the formation of an electrical double layer at the interface between the electrode and the LC layer. In the samples containing ionic impurity such as sodium and halogen ions which are contaminated in the synthetic processes, additional peaks other than the peak originated from the ferroelectric polarization inversion are observed in the triangular wave measurements. However, no additional peaks associated with ionic transport were observed in the SmC* or isotropic phases. The detection limit of the current peaks in the triangular wave experiment was about 1 $nCcm^{-2}$. The charge on the electrodes formed by ionic impurities should be lower than 1 $nCcm^{-2}$, which is two orders of magnitude lower than the spontaneous polarization in the SmC* phase of compound **1**.

The anomalous photovoltaic effect can produce a higher voltage than the band gap of the semiconductors. Production of thin films of the ferroelectric phenylterthiophene derivatives and measurements of the photovoltaic effect in the thin film states are in progress.

Conclusions

Phenylterthiophene derivatives bearing a decenyl group, disiloxane chain, and tetrasiloxane ring were synthesized. They exhibited hole mobilities on the order of 10^{-4} $cm^{2}V^{-1}s^{-1}$ in the SmC* phase. Even the compound bearing a bulky cyclotetrasiloxane ring exhibited an enantiotropic SmC* phase. The spontaneous polarization in the SmC* phases exceed 100 $nCcm^{-2}$. Compound **1** exhibited a photovoltaic effect based on the internal electric field produced by spontaneous polarization.

Acknowledgements

This study was financially supported by the Japan Security Scholarship Foundation, the Ogasawara Foundation, a Grant-in-Aid for Scientific Research on Innovative Areas (Coordination Programming, no. 24108729 and Element-Block Polymers, no. 25102533) from the Ministry of Education, Culture, Sports, Science and Technology (MEXT), a Grant-in-Aid for Scientific Research (B) (no. 22350080) from the Japan Society for the Promotion of Science (JSPS), the Iwatani Naoji Foundation, the Asahi Glass Foundation, and the Murata Science Foundation. The authors thank T. Kusunose at Kagawa University for help with the DSC measurements. We also thank Prof. N. Tamaoki of Hokkaido University, Prof. T. Kato of the University of Tokyo, and Dr. Emi Uchida of the National Institute of Advanced Materials Science and Technology for fruitful discussions.

Notes and references

[a] Department of Advanced Materials Science, Faculty of Engineering, Kagawa University, 2217-20 Hayashi-cho, Takamatsu, Kagawa 761-0396 Japan. Fax: (+81)-87-864-2411; Tel: (+81)-87-864-2411; E-mail: m-funa@eng.kagawa-u.ac.jp

[b] Health Research Institute, National Institute of Advanced Industrial Science and Technology, 2217-14 Hayashi-cho, Takamatsu, Kagawa 761-0395, Japan.

1 (a) W. Pisula, M. Zorn, J. Y. Chang, K. Müllen, R. Zentel, *Macromol. Rapid Commun*., 2009, **30**, 1179-1202. (b) Y. Shimizu, K. Oikawa, K. Nakayama, D. Guillon, *J. Mater. Chem*. 2007, **17**, 4223-4229. (c) M. O'Neill, S. M. Kelly, *Adv. Mater*., 2011, **23**, 566-584. (d) M. Funahashi, H. Shimura, M. Yoshio, T. Kato, *Structure and Bonding*, 2008, **128**, 151-179. (e) M. Funahashi, T. Yasuda, T. Kato, *Handbook of Liquid Crystals 2nd Ed.* Wiley-VCH, 2014, **8**, 675-708.

2 (a) D. Adam, F. Closs, T. Frey, D. Funhoff, D. Haarer, H. Ringsdorf, P. Schuhmacher, K. Siemensmeyer, *Phys. Rev. Lett*., 1993, **70**, 457-460. (b) N. Boden, R. J. Bushby, J. Clements, B. Movaghar, K. J. Donovan, T. Kreouzis, *Phys. Rev. B*, 1995, **52**, 13274-13280. (c) A. M. van de Craats, J. M. Warman, A. Fechtenkötter, J. D. Brand, M. A. Harbison, K. Müllen, *Adv. Mater*., 1999, **11**, 1469-1472. (d) M. Ichihara, A. Suzuki, K. Hatsusaka, K. Ohta, *Liq. Cryst*., 2007, **34**, 555-567. (e) K. Ban, K. Nishikawa, K. Ohta, A. M. van de Craats, J. M. Warman, I. Yamamoto, H. Shirai, *J. Mater. Chem*., 2001, **11**, 321-331. (f) A. Demenev, S. H. Eichhorn, T. Taerum, D. Perepichka, S. Patwardhan, F. C. Grozema, L. D. A. Siebbeles, *Chem. Mater*., 2010, **22**, 1420-1428. (g) I. Bleyl, C. Erdelen, H.-W. Schmidt, D. Haarer, *Phil. Mag. B*, 1999, **79**, 463-475. (h) J. Simmerer, B. Glüsen, W. Paulus, A. Kettner, P. Schuhmacher, D. Adam, K.-H. Etzbach, K. Siemensmeyer, J. H. Wendorf, H. Ringsdorf, D. Haarer, *Adv. Mater*., 1996, **8**, 815-819.

3 (a) M. Funahashi, J. Hanna, *Phys. Rev. Lett*., 1997, **78**, 2184-2187. (b) M. Funahashi, J. Hanna, *Appl. Phys. Lett*., 2000, **76**, 2574-2576. (c) M. Funahashi, J. Hanna, *Adv. Mater*., 2005, **17**, 594-598. (d) K. Oikawa, H. Monobe, J. Takahashi, K. Tsuchiya, B. Heinrich, D. Guillon, Y. Shimizu, *Chem. Commun*., 2005, 5337-5339. (e) A. Matsui, M. Funahashi, T. Tsuji, T. Kato, *Chem. Eur. J*., 2010, **16**, 13465-13472. (f) H. Aboubakr, M.-G. Tamba, A. K. Diallo, C. Videlot-Ackermann, L. Belec, O. Siri, J.-M. Raimundo, G. H. Mehl, H. Brisset, *J. Mater. Chem*., 2012, **22**, 23159-23168. (g) M. Funahashi, F. Zhang, N. Tamaoki, J. Hanna, *ChemPhysChem*, 2008, **9**, 1465-1473. (h) M. Funahashi, T. Ishii, A. Sonoda, *ChemPhysChem*, 2013, **14**, 2750-2758.

4 (a) A. J. J. M. van Breemen, P. T. Herwig, C. H. T. Chlon, J. Sweelssen, H. F. M. Schoo, S. Setayesh, W. M. Hardeman, C. A. Martin, D. M. de Leeuw, J. J. P. Valeton, C. W. M. Bastiaansen, D. J. Broer, A. R. Popa-Merticaru, S. C. J. Meskers, *J. Am. Chem. Soc*., 2006, **128**, 2336-2345. (b) M. Funahashi, F. Zhang, N. Tamaoki, *Adv. Mater*., 2007, **19**, 353-358. (c) W. Pisula, A. Menon, M. Stepputat, I. Lieberwirth, U. Kolb, A. Tracz, H. Sirringhaus, T. Pakula, K. Müllen, *Adv. Mater*., 2005, **17**, 684-689. (d) M. Funahashi, *Polym. J*., 2009, **41**, 459-469. (e) F. Zhang, M. Funahashi, N. Tamaoki, *Org. Electr*., 2010, **11**, 363-368.

5 (a) T. Hassheider, S. A. Benning, H.-S. Kitzerow, M.-F. Achard, H. Bock, *Angew. Chem., Int. Ed*., 2001, **40**, 2060-2063. (b) M. P. Aldred, A. E. A. Contoret, S. R. Farrar, S. M. Kelly, D. Mathieson, M. O'Neill, W. C. Tsoi, P. Vla-chos, *Adv. Mater*., 2005, **17**, 1368-1372. (c) S. A. Benning, R. Oesterhaus, H.-S. Kitzerow, *Liq. Cryst*., 2004, **31**, 201-205. (d) M. W. Lauhof, S. A. Benning, H.-S. Kitzerow, V. Vill, F. Scheliga, E. Thorn-Csányi, *Synth. Met*., 2007, **157**, 222-227.

6 (a) T. Hori, Y. Miyake, N. Yamasaki, H. Yoshida, A. Fujii, Y. Shimizu, M. Ozaki, *Appl. Phys. Exp*., 2010, **3**, 101602. (b) W. Shin, T. Yasuda, G. Watanabe, Y. S. Yang, C. Adachi, *Chem. Mater*., 2013, **25**, 2549-2556.

7 (a) T. Kato, T. Yasuda, Y. Kamikawa, M. Yoshio, *Chem. Commun*., **2009**, 729-739. (b) M. Funahashi, *J. Mater. Chem. C*, in press (2014); (c) T. Yasuda, H. Ooi, J. Morita, Y. Akama, K. Minoura, M. Funahashi, T. Shimomura, T. Kato, *Adv. Funct. Mater*., 2009, **19**, 411-419. (d) S. Yazaki, M. Funahashi, T. Kato, *J. Am. Chem. Soc*., 2008, **130**, 13206-13207. (e) S. Yazaki, M. Funahashi, J. Kagimoto, H. Ohno, T. Kato, *J. Am. Chem. Soc*., 2010, **132**, 7702-7708. (e) M. Yoneya, *Chem. Rec*., 2011, **11**, 66-76.

8 (a) M. Funahashi, A. Sonoda, *Org. Electr*., 2012, **13**, 1633-1640. (b) M. Funahashi, A. Sonoda, *J. Mater. Chem*., 2012, **22**, 25190-25197. (c) M. Funahashi, A. Sonoda, *Dalton Trans*., 2013, **42**, 15987-15994. (d) M. Funahashi, M. Yamaoka, K. Takenami, A. Sonoda, *J. Mater. Chem. C*, 2013, **1**, 7872-7878. (e) M. Funahashi, T. Ishii, A. Sonoda, *Phys. Chem. Chem. Phys*., 2014, **16**, 7754-7763.

9 (a) C. Y. Young, R. Pindak, N. A. Clark, R. B. Meyer, *Phys. Rev. Lett*., 1978, **40**, 773-776. (b) N. A. Clark, S. T. Lagerwall, *Appl. Phys. Lett*., 1980, **36**, 899-901. (c) S. T. Lagerwall, I. Dahl, *Mol. Cryst. Liq. Cryst*., 1984, **114**, 151-187. (d) W. J. A. M. Hartmann, *Ferroelectrics*, 1991, **122**, 1-26.

10 K. Kogo, H. Maeda, H. Kato, M. Funahashi, J. Hanna, *Appl. Phys. Lett*., 1999, **75**, 3348-3350.

11 (a) Y. Zhang, Y. Liu, Z. L. Wang, *Adv. Mater*., 2011, **23**, 3004-3013. (b) T. Choi, S. Lee, Y. J. Choi, V. Kiryukhin, S.-W. Cheong, *Science*, 2009, **324**, 63-66. (c) I. Grinberg, D. V. West, M. Torres, G. Gou, D. M. Stein, L. Wu, G. Chen, E. M. Gallo, *Nature*, 2013, **503**, 509-517.

12 (a) H. Sasabe, T. Nakayama, K. Kumazawa, S. Miyata, E. Fukuda, *Polym. J*., 1981, **13**, 967-973. (b) A. Sugita, K. Suzuki, S. Tasaka, *Phys. Rev. B*, 2004, **69**, 212201.

13 (a) J. Watanabe, Y. Nakata, K. Simizu, *J. Phys. II*, 1994, **4**, 581-588. (b) T. Niori, T. Sekine, J. Watanabe, T. Furukawa, H. Takezoe, *J. Mater. Chem*., 1996, **6**, 1231-1233. (c) G. Pelzl, S. Diels, W. Weissflog, *Adv. Mater*., 1999. **11**, 707-724. (d) C. F. C. Fitié, W. S. C. Roelofs, M. Kemerink, R. P. Sijbesma, *J. Am. Chem. Soc*., 2010, **132**, 6892-6893. (e) D. Miyajima, F. Araoka, H. Takezoe, J. Kim, K. Kato, M. Takata, T. Aida, *J. Am. Chem. Soc*., 2010, **132**, 8530-8531. (f) D. Miyajima, F. Araoka, H. Takezoe, K. Kato, M. Takata, T. Aida, *Science*, 2012, **336**, 209-213.

14 (a) R. G. Kepler, *Phys. Rev*., 1960, **119**, 1226-1229. (b) W. E. Spear, *J. Non-Cryst. Solid*, 1968, **1**, 197-214.

15 (a) D. L. Hughes, *Org. Prep. Proced. Int*., 1996, **28**, 127-164. (b) N. Miyaura, A. Suzuki, *Chem. Rev*., 1995, **95**, 2457–2483.

16 (a) G. H. Mehl, J. Goodby, *Angew. Chem*., *Int. Ed. Engl*., 1996, **35**, 2641-2643. (b) I. M. Saez, J. W. Goodby, R. M. Richardson. *Chem. Eur. J*., 2001, **7**, 2758-2764. (c) J. Newton, H. Coles, P. Hodge, J. Hannington, *J. Mater. Chem*., 1994, **4**, 869-874. (d) J. C. Roberts, N. Kapernaum, F. Giesselmann, R. P. Lemieux, *J. Am. Chem. Soc*., 2008, **130**, 13842-13843. (e) D. Apreutesei, G. Mehl, *J. Mater. Chem*., 2007, **17**, 4711-4715.

17 B. D. Karstedt, *U.S. Patent* 3,775,452, 1973.

18 (a) A. de Vries, *Mol. Cryst. Liq. Cryst*., 1985, **131**, 125-145. (b) S. Diele, D. Jaeckel, D. Demus, H. Sackmann, *Cryst. Res. Tech*., 1982, **17**, 1591-1598. (c) P. A. C. Gane, A. J. Leadbetter, *J. Phys. C: Solid Stat. Phys*., 1983, **16**, 2059-2007.

19 (a) H. Bässler, *Phys. Status Solidi B*, 1993, **175**, 15-56. (b) M. van der Auweraer, F. C. Schryver, P. M. Borsenberger, H. Bässler, *Adv. Mater*. 1994, **6**, 199-213. (c) A. Köhler, H. Bässler, *Top. Curr. Chem*., 2012, **312**, 1-66. (d) R. Goehoorn, P. A. Bobbert, *Phys. Status Solidi A*, 2012, **209**, 2354-2377. (e) T. Nagase, K. Kishimoto, H. Naito, *J. Appl. Phys*., 1999, **86**, 5026-5035.

20 (a) M. A. Palenberg, R. J. Silbey, M. Malagoli, J.-L. Brédas, *J. Chem. Phys*., 2000, **112**, 1541-1546. (b) V. Duzhko, A. Semyonov, R. J. Twieg, K. D. Singer, *Phys. Rev. B*, 2006, **73**, 064201. (c) I. Shiyanovskaya, K. D. Singer, R. J. Twieg, L. Sukhomlimova, V. Gettwert, *Phys. Rev. E*, 2002, **65**, 041715. (d) T. Kreouzis, K. J. Donovan, N. Boden, R. J. Bushby, O. R. Lozman, Q. Liu, *J. Chem. Phys*., 2001, **114**, 1797-1802.

21 (a) A. Hirao, H. Nishizawa, *Phys. Rev. B*, 1996, **54**, 4755-4761. (b) T. Nagase, H. Naito, *J. Appl. Phys*. 2000, **88**, 252-259. (c) H. Iino, J. Hanna, R. J. Bushby, B. Movaghar, B. J. Whitaker, *J. Appl. Phys*., 2006, **100**, 043716.

Table of contents